Integrated Segmentation of Brain Tumor Images

For Radiotherapy and Neurosurgery

Stefan Bauer[a], Huanxiang Lu[a], Christian P. May[a,b], Lutz-P. Nolte[a], Philippe Büchler[a], Mauricio Reyes[a]

[a] Institute for Surgical Technology and Biomechanics, University of Bern, Switzerland

[b] RMS Foundation, Bettlach, Switzerland

Short title : Integrated Segmentation of Brain Tumor Images

Contact:

Stefan Bauer

ISTB, University of Bern

Stauffacherstr. 78 3014 Bern Switzerland

stefan.bauer@istb.unibe.ch

phone: +41 31 631 5952

fax: +41 31 631 5960

Abstract

Segmentation of brain tumor images is an important task in diagnosis and treatment planning for cancer patients. To achieve this goal with standard clinical acquisition protocols, conventionally, either classification algorithms are applied on multimodal MR images or atlas-based segmentation is used on a high-resolution mono-modal MR image. These two approaches have been commonly regarded separately. We propose to integrate all the available imaging information into one framework in order to be able to use the information gained from the tissue classification of the multimodal images to perform a more precise segmentation on the high-resolution mono-modal image by atlas-based segmentation. For this, we combine a state of the art regularized classification method with an enhanced version of an atlas-registration approach including multi-scale tumor-growth modeling. This contribution offers the possibility to simultaneously segment subcortical structures in the patient by warping the respective atlas labels, which is important for neurosurgical planning and radiotherapy planning.

Keywords: Brain Tumor, Glioma, Atlas-based Segmentation, Tumor-growth Modeling, Multimodal Image Analysis

Introduction

The segmentation of tumor-bearing brain images is a highly relevant, but difficult problem in medical image analysis (Angelini et al., 2007). It is desirable to be able to perform this task in an automatized way because manual segmentations are time-consuming and tedious. Additionally, the reproducibility of manual segmentations is very limited, as reported in (Mazzara, Velthuizen, Pearlman, Greenberg, & Wagner, 2004).

In a clinical environment, usually two different kinds of datasets are acquired from brain tumor patients: a multimodal dataset consisting of T_1, $T_{1contrast}$, T_2 and T_{2flair} weighted magnetic resonance images (MRI) for diagnosis and treatment monitoring. This dataset is very anisotropic with high intra-slice resolution but large inter-slice spacings. An additional isotropic $T_{1(contrast)}$-weighted dataset is used for neurosurgery and radiotherapy planning. An example of the four anisotropic images from the multimodal dataset, and the isotropic image from the mono-modal dataset are depicted in figure 1.

Figure 1

Along with the two different kinds of data sets available, the current segmentation methods can also be divided into two different categories: In most cases, classification methods with some degree of spatial regularization are employed for the segmentation of the multimodal dataset (Bauer, Nolte, & Reyes, 2011; Verma et al., 2008; Wels et al., 2008), while atlas-based segmentation is an established way for segmenting the mono-modal image (Bach Cuadra et al., 2006; Bauer, May, et al., 2012; Deeley et al., 2011; Gooya, Biros, & Davatzikos, 2011; Gooya,

Pohl, Bilello, Biros, & Davatzikos, 2011; Isambert et al., 2008; Zacharaki, Hogea, Shen, Biros, & Davatzikos, 2009). Using atlas-based segmentation on the high-resolution mono-modal image is attractive thanks to its robustness and its versatile usability because it allows DTI maps or subcortical label maps to be overlaid on the patient image, which is important information in neurosurgery and radiotherapy. Most atlas-based segmentation methods establish initial correspondence between a healthy atlas and a pathologic patient image by seeding the atlas with a patient-specific tumor prior, which is often based on a tumor-growth model. The deformation field obtained after non-rigid registration of the modified atlas to the patient image, can be used for warping the atlas label image, thus obtaining an implicit segmentation of the patient image. The shortcomings of most current approaches include the need for a manual segmentation of the tumor area as an input. Additionally, they do not make use of the full power of atlas-based segmentation because they only output tissue label maps, but no other structures of interest, which are important for radiotherapy or neurosurgical planning.

Segmentation of the tumor and its different sub-regions is more reliable when based on the anisotropic multimodal images due to specific information from each modality, while segmentation of the healthy structures around the tumor is more accurate when based on the high-resolution mono-modal images thanks to more structural details. So far, both datasets and the two different approaches for segmentation have been mostly regarded separately and an integrated combination, which makes selective use of all the image data available is still missing. An integration of the two methods would be attractive because atlas-based segmentation of the

mono-modal image needs a segmentation of the tumor as an input and could therefore benefit from information obtained from the segmentation of the multi-modal images.

Methods

In this contribution, two different methods for segmentation of tumor-bearing brain images are combined to form an integrated approach, which makes use of all the imaging data available: First, tissue classification is performed on the multimodal images. This serves as an initialization for a method combining tumor-growth modeling with atlas registration for segmenting the isotropic high-resolution mono-modal image.

We use a fully automatic classification method with integrated hierarchical regularization, based on (Bauer et al., 2011) for segmenting the multimodal images. Intensity and texture features of individual voxels from all modalities are classified by a support vector machine (SVM). Subsequently, a hierarchical conditional random field (CRF) regularization is applied in order to take spatial information and prior knowledge into account. The output of the segmentation method are the healthy and pathologic regions, whereas the healthy part is subdivided into cerebrospinal fluid (CSF), gray matter (GM), white matter (WM) and the pathologic part is subdivided into necrotic tissue, active tumor and perifocal edema.

This information about the tumor tissue classes is used as an input to the atlas-based segmentation of the isotropic mono-modal image for neurosurgery and radiotherapy planning. The method for atlas-based segmentation is based on a similar idea as the one proposed in (Bauer, May, et al., 2012). The problem in atlas-based segmentation of tumor-bearing brain images is the missing tumor prior in the atlas. This can be solved by establishing initial correspondence between the healthy atlas and the pathologic patient image employing a tumor-growth model prior to the non-rigid registration step. In order to be able to grow a patient-specific tumor in the atlas, location and extent of the tumor have to be known. After affine registration of the atlas to the patient image, we obtain this information from the segmentation of the multimodal images, where necrotic and active tumor tissue are combined into one tumor class. In the atlas, a physically realistic seed for tumor growth modeling is automatically chosen in the center of mass of the patient tumor. Then, a multi-scale tumor growth model is used to grow a tumor in the atlas and deform the surrounding tissues in a biomechanically justified way. The method is based on a sophisticated bio-physio-mechanical model, which incorporates multiple scales, from the cellular up to the bio-mechanical level(May, Kolokotroni, Stamatakos, & Büchler, 2011). Cell proliferation and apoptosis is modeled by an oncosimulator and this information is coupled with an Eulerian finite element method (FEM) in order to compute the preferred direction of tumor growth. The biomechanical problem is solved using a linear elastic tissue model. The direction of tumor growth is determined according to equation (1), where we assume that newly generated biological cells follow the direction $\mathbf{d}$ of least pressure in the surrounding tissues, which corresponds to the negative gradient. For this, the pressure p is given as the trace of the stress tensor $\boldsymbol{\sigma}$.

$$\mathbf{d} = -\frac{\nabla p}{\|\nabla p\|} \qquad (1)$$

After establishing correspondence between atlas and patient image by tumor-growth modeling, a final non-rigid registration step is applied using a Demons approach. However, in contrast to (Bauer, May, et al., 2012) we do not use the standard Diffeomorphic Demons (Vercauteren, Pennec, Perchant, & Ayache, 2009), but we use a variant proposed in (Lu et al., 2010), which employs pointwise mutual information (PMI) as similarity metric. Given two images F and M, the Demons registration model can be summarized by equation (2)

$$E(\mathbf{s}) = \mathrm{Sim}(F, M \circ \mathbf{s}) + \alpha \cdot \mathrm{Reg}(\mathbf{s}) \qquad (2)$$

where $\mathrm{Sim}(F, M \circ \mathbf{s})$ is the criterium measuring the similarity between the fixed image F and the moving image M, which has been warped by the deformation field $\mathbf{s}$. $\mathrm{Reg}(\mathbf{s})$ is a regularization term to restrict the deformation. In our case, the similarity term in equation (2) is based on the pointwise mutual information metric, where we assume that each voxel x has a certain contribution to the global mutual information. We compute the mutual information MI based on the probabilities P according to equation (3)

$$\mathrm{MI} = \frac{1}{N} \sum_x \log\left(\frac{P(i_F(x), i_M(x))}{P(i_F(x)) \cdot P(i_M(x))} \right) \qquad (3)$$

N is the total number of voxels in the image, i_F and i_M are the intensities of the fixed and moving image respectively.

Although perifocal edema cannot be reliably detected in T_1-weighted MR images, it can lead to subtle changes of tissue intensities. Therefore, a similarity metric based on mutual information will be more robust in handling these confounding effects than the sum of squared differences (SSD) metric, which is normally used.

The deformation field, which is finally obtained, is used to warp the tissue label map as well as the subcortical label map from the atlas to the patient image. This allows for an implicit segmentation of the relevant structures in the patient image.

Results

We use a publicly available atlas (Rohlfing, Zahr, Sullivan, & Pfefferbaum, 2010), which includes structural information, tissue label maps and subcortical label maps. The proposed method was evaluated on 10 datasets from the ContraCancrum database (Marias et al., 2011). The database contains multi-modal MR images (T_1, $T_{1contrast}$, T_2 and T_{2flair}) in axial acquisition of various anisotropic resolutions with large slice spacing (less than 1mm in-plane, between 3.5mm and 5.5mm out-of-plane). The high-resolution $T_{1contrast}$ images for neurosurgery planning have either an isotropic resolution of 1mm or 1mm in-slice spacing and 2mm between slices. In a preprocessing step, the different modalities of each patient are all rigidly registered with the structural T_1 image and the skull is automatically removed using (Bauer, Fejes, & Reyes, 2012).

The most important steps of the workflow are summarized in figure (2) on an axial slice of one patient: (a) shows the skull-stripped isotropic $T_{1contrast}$-weighted image of the patient and (b) depicts an overlay of the tumor segmentation, which was obtained from the tissue classification on the multimodal dataset by combining necrotic and active tumor region. This information is used to automatically seed the affinely registered atlas image with a physically realistic tumor seed in the center of mass of the patient tumor (c). Figures (2) (d) and (e) show an intermediate step and the final step of the multi-scale tumor growth model deforming the surrounding tissues based on their bio-mechanical properties. Finally, the modified atlas is warped to the patient image by non-rigid registration using an intensity-based pointwise mutual information metric (f). Implicit segmentation of the patient image is achieved by propagation of the tissue label map (g) and the subcortical label map (h), onto which the edema region is overlaid as a blue line.

Figure 2

Figure (3) shows the results for the segmentation of subcortical structures on two more patient images. Additionally to these labels, an outline of the edema region (overlaid as a blue line), obtained from the multimodal tissue classification, can help the clinician in decision-making.

Figure 3

Quantitative evaluation has been performed using Dice similarity coefficient and is summarized in table 1. The Dice coefficient can range between 0 and 1, with 0 indicating no overlap and 1 indicating perfect overlap. The ground-truth for the tissue segmentation was obtained semi-manually, where tissues were pre-segmented using FSL[1], the tumor delineation was done

[1] www.fmrib.ox.ac.uk/fsl

manually by a trained expert and the segmentation result was manually post-processed and corrected where necessary. In order to provide quantitative evaluation of the subcortical segmentation as well, one exemplary region (left and right caudate nuclei) was manually segmented on all patients. The average Dice coefficient for the tissue segmentation on 10 datasets was 0.41 for CSF, 0.65 for gray matter and 0.72 for white matter, whereas tumor tissue had an average Dice coefficient of 0.64. The left caudate nuclei had an average Dice coefficient of 0.58 and the right caudate nuclei of 0.45. The results of the healthy tissue segmentations are in the range of the accuracy of standard segmentation algorithms. The accuracy of the tumor segmentation still needs to be improved for clinical application, however it already comes close to accuracies achieved in inter-observer studies of manual segmentations by (Mazzara et al., 2004). Achieving accurate segmentations of small subcortical structures is more challenging due to the fact that it is difficult to define their borders. But the currently achieved accuracy might be sufficient for structures, which are not in the immediate vicinity of the tumor during resection or radiotherapy.

Table 1

Computation time ranged from 6 hours to 48 hours on a single CPU. The vast majority of time was spent for the multi-scale tumor growth model. Computation speed depended mostly on the size of the tumor because larger tumors require more growth iterations. The program is currently running on a single core of a standard CPU. The time-consuming computation of the bio-mechanical deformations during tumor growth modeling can be parallelized, which offers a significant potential for speed-up when running on a cluster.

Discussion & Conclusion

We present an integrated approach for segmentation of tumor-bearing brain images, which considers and combines all the image data available from the standard clinical acquisition protocols. It offers the potential for fully automatic segmentation of tumor-bearing brain images. The presented method is able to not only delineate tissue maps, but also subcortical structures in a sophisticated way from tumor-bearing brain images, by incorporating tumor-growth modeling and non-rigid registration. The segmentation of subcortical structures in brain tumor images can have important implications in neurosurgery and radiotherapy planning. Additionally, the presented approach has the potential to warp any other available atlas map (e.g. DTI) to the patient image and use it for further processing.

The only method which achieves a similar level of integration was presented in (Gooya, Biros, et al., 2011). However, in our approach, the final registration can directly depend on the image intensities instead of probability maps, because the pointwise mutual information metric is more robust to intensity variations than the standard Demons registration. The results for the validation of tissue segmentation are in a similar range as recently reported by (Gooya, Biros, et al., 2011), although slightly lower. However, different data was used, which makes a direct comparison impossible. Furthermore, tumor growth-modeling was applied on a subsampled dataset (2mm isotropic resolution) in order to cope with the computational requirements. We expect an

increase in accuracy when using the full resolution. In contrast to (Gooya, Biros, et al., 2011), in this study we are able to make use of the full potential of atlas-based segmentation by not only segmenting tissue classes, but also subcortical structures and combining both outcomes.

It should be acknowledged that the accuracy of the final segmentation result is currently confined by the accuracy of tumor segmentation in the multimodal dataset and the transfer of this region to the isotropic mono-modal dataset by linear registration, which has to cope with partial volume effects in the anisotropic images. Also, multifocal lesions cannot be handled explicitly yet by the current implementation. The clinical applicability of the method is still limited due to the heavy computational requirements.

Acknowledgements

We would like to thank Professor Georgios Stamatakos and his team at NTUA, Greece, for sharing the code of the cellular-level oncosimulator. This research was partially funded by the European Union within the ContraCancrum project (FP7 - IST-223979) and it was also partially funded by the Swiss National Science Foundation within the framework of the NCCR Co-Me.

References

Angelini, E. D., Clatz, O., Mandonnet, E., Konukoglu, E., Capelle, L., & Duffau, H. (2007). Glioma Dynamics and Computational Models: A Review of Segmentation, Registration, and In Silico Growth Algorithms and their Clinical Applications. *Current Medical Imaging Reviews*, *3*(4), 262–276. doi:10.2174/157340507782446241

Bach Cuadra, M., De Craene, M., Duay, V., Macq, B., Pollo, C., & Thiran, J.-P. (2006). Dense deformation field estimation for atlas-based segmentation of pathological MR brain images. *Computer methods and programs in biomedicine*, *84*(2-3), 66–75. doi:10.1016/j.cmpb.2006.08.003

Bauer, S., Fejes, T., & Reyes, M. (2012). *A Skull-Stripping Filter for ITK*.

Bauer, S., May, C., Dionysiou, D., Stamatakos, G., Buchler, P., & Reyes, M. (2012). Multi-Scale Modeling for Image Analysis of Brain Tumor Studies. *IEEE Transactions on Biomedical Engineering*, *59*(1), 25–29. doi:10.1109/TBME.2011.2163406

Bauer, S., Nolte, L.-P., & Reyes, M. (2011). Fully automatic segmentation of brain tumor images using support vector machine classification in combination with hierarchical conditional random field regularization. In G. Fichtinger, A. Martel, & T. Peters (Eds.), *MICCAI ... International Conference on Medical Image Computing and Computer-Assisted Intervention* (Vol. 14, pp. 354–61). Toronto: Springer Berlin Heidelberg. doi:10.1007/978-3-642-23626-6_44

Deeley, M. A., Chen, A., Datteri, R., Noble, J. H., Cmelak, A. J., Donnelly, E. F., Malcolm, A. W., et al. (2011). Comparison of manual and automatic segmentation methods for brain structures in the presence of space-occupying lesions: a multi-expert study. *Physics in medicine and biology*, *56*(14), 4557–77. doi:10.1088/0031-9155/56/14/021

Gooya, A., Biros, G., & Davatzikos, C. (2011). Deformable registration of glioma images using em algorithm and diffusion reaction modeling. *IEEE transactions on medical imaging*, *30*(2), 375–90. doi:10.1109/TMI.2010.2078833

Gooya, A., Pohl, K., Bilello, M., Biros, G., & Davatzikos, C. (2011). Joint Segmentation and Deformable Registration of Brain Scans Guided by a Tumor Growth Model. In G. Fichtinger, A. Martel, & T. M. Peters (Eds.), *Medical Image Computing and Computer-Assisted Intervention–MICCAI 2011* (pp. 532–540). Toronto: Springer LNCS. doi:10.1007/978-3-642-23629-7_65

Isambert, A., Dhermain, F., Bidault, F., Commowick, O., Bondiau, P.-Y., Malandain, G., & Lefkopoulos, D. (2008). Evaluation of an atlas-based automatic segmentation software for

the delineation of brain organs at risk in a radiation therapy clinical context. *Radiotherapy and oncology□: journal of the European Society for Therapeutic Radiology and Oncology*, *87*(1), 93–9. doi:10.1016/j.radonc.2007.11.030

, A., Weber, S., Sakurai, Y., Yamagata, H., & Cattin, P. (2010). Multi-modal diffeomorphic demons registration based on point-wise mutual information. *Biomedical Imaging: From Nano to Macro, 2010 IEEE International Symposium on* (pp. 372–375). IEEE.

Marias, K., Dionysiou, D., Sakkalis, V., Graf, N., Bohle, R. M., Coveney, P. V., Wan, S., et al. (2011). Clinically driven design of multi-scale cancer models: the ContraCancrum project paradigm. *Journal of the Royal Society - Interface Focus*, *1*(3), 450–461. doi:10.1098/rsfs.2010.0037

May, C. P., Kolokotroni, E., Stamatakos, G. S., & Büchler, P. (2011). Coupling biomechanics to a cellular level model: an approach to patient-specific image driven multi-scale and multi-physics tumor simulation. *Progress in biophysics and molecular biology*, *107*(1), 193–9. doi:10.1016/j.pbiomolbio.2011.06.007

Mazzara, G. P., Velthuizen, R. P., Pearlman, J. L., Greenberg, H. M., & Wagner, H. (2004). Brain tumor target volume determination for radiation treatment planning through automated MRI segmentation. *International journal of radiation oncology, biology, physics*, *59*(1), 300–12. doi:10.1016/j.ijrobp.2004.01.026

Rohlfing, T., Zahr, N. M., Sullivan, E. V., & Pfefferbaum, A. (2010). The SRI24 multichannel atlas of normal adult human brain structure. *Human brain mapping*, *31*(5), 798–819. doi:10.1002/hbm.20906

Vercauteren, T., Pennec, X., Perchant, A., & Ayache, N. (2009). Diffeomorphic demons: efficient non-parametric image registration. *NeuroImage*, *45*(1 Suppl), S61–72. doi:10.1016/j.neuroimage.2008.10.040

Verma, R., Zacharaki, E. I., Ou, Y., Cai, H., Chawla, S., Lee, S.-K., Melhem, E. R., et al. (2008). Multiparametric tissue characterization of brain neoplasms and their recurrence using pattern classification of MR images. *Academic radiology*, *15*(8), 966–77. doi:10.1016/j.acra.2008.01.029

Wels, M., Carneiro, G., Aplas, A., Huber, M., Hornegger, J., & Comaniciu, D. (2008). A discriminative model-constrained graph cuts approach to fully automated pediatric brain tumor segmentation in 3-D MRI. *Medical image computing and computer-assisted intervention□: MICCAI ... International Conference on Medical Image Computing and Computer-Assisted Intervention*, *11*(Pt 1), 67–75.

Zacharaki, E. I., Hogea, C. S., Shen, D., Biros, G., & Davatzikos, C. (2009). Non-diffeomorphic registration of brain tumor images by simulating tissue loss and tumor growth. *NeuroImage*, *46*(3), 762–774. doi:10.1016/j.neuroimage.2009.01.051

Figures:

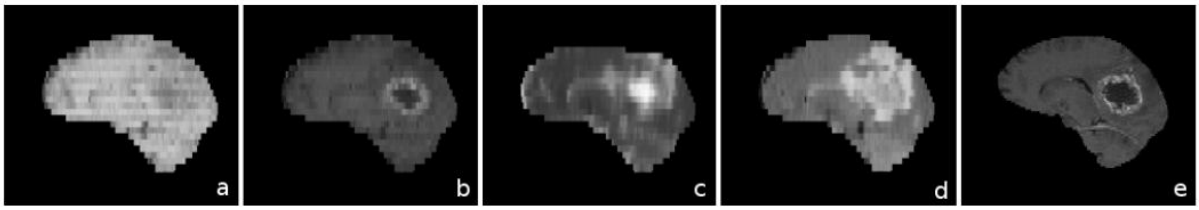

Figure 1:

One reconstructed sagittal slice of the multimodal dataset with anisotropic resolution (T_1 (a), $T_{1contrast}$ (b), T_2 (c) and T_{2flair} (d)) and one sagittal slice of the isotropic $T_{1contrast}$-weighted dataset (e) from the same patient. When not integrated with the isotropic $T_{1contrast}$ -weighted dataset, the four multimodal images on the left cannot be used for surgery or radiotherapy planning due to their large slice spacing.

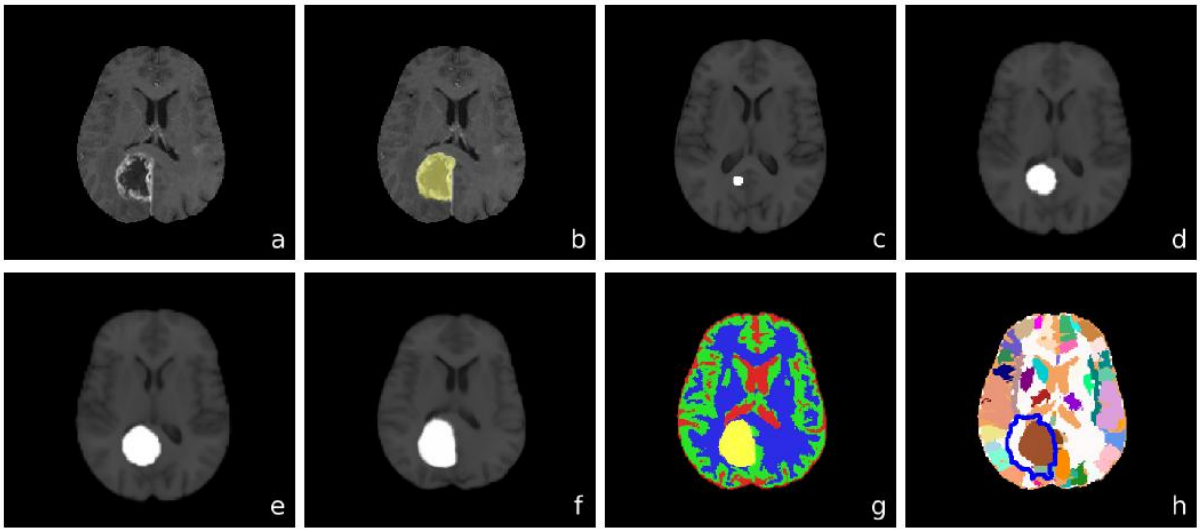

Figure 2:

Workflow shown step by step on one axial slice: (a) isotropic $T_{1contrast}$ patient image, (b) multimodal tumor segmentation, (c) seeded atlas, (d) deformed atlas during intermediate step of multi-scale tumor growth modeling, (e) deformed atlas after final step of multi-scale tumor growth modeling, (f) atlas after final non-rigid registration step, (g) tissue label map of segmented patient image, (h) subcortical label map of segmented patient image (solid tumor in brown) including an outline of the edema region (blue line).

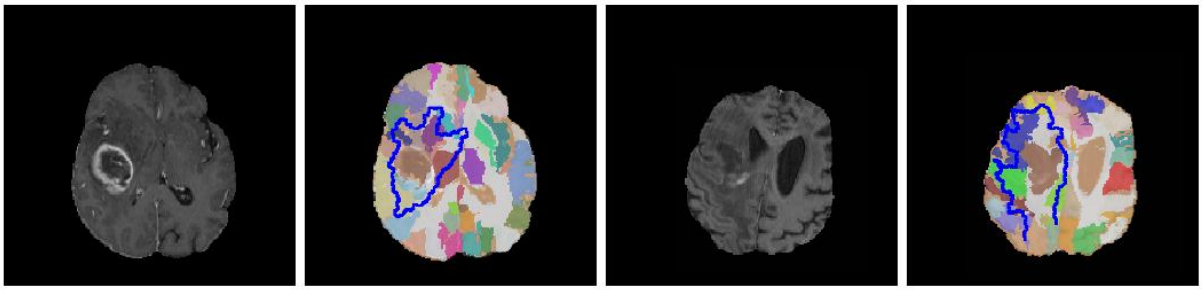

Figure 3:

Segmentation results shown on an axial slice of two different patient images. In addition to the subcortical labels from atlas-based segmentation (solid tumor in brown), an outline of the edema region, based on the multimodal tissue classification method, is overlaid as a blue line.

Tables:

Table 1:

Dice similarity coefficients for cerebrospinal fluid (CSF), gray matter (GM), white matter (WM), left/right caudate nuclei ($CN_{l/r}$) and tumor, achieved by the proposed method on the 10 datasets under study.

	CSF	GM	WM	CN_l	CN_r	Tumor
Mean	0.41	0.65	0.72	0.58	0.45	0.64
Standard Deviation	0.06	0.07	0.06	0.20	0.16	0.14